Complex Band Structures: From Parabolic to Elliptic Approximation

Ximeng Guan, *Member, IEEE*, Donghyun Kim, Krishna C. Saraswat, *Fellow, IEEE*, and H.-S. Philip Wong, *Fellow, IEEE*

***Abstract*—We show that the conventional nonparabolic approximation of real band structures can be modified and generalized to approximate the complex band structures of common semiconductors with a significant improvement of accuracy against the parabolic approximation. The improvement is due to the inherent elliptic nature of the complex band structures in the vicinity of the bandgap, which has a critical impact on the band-to-band tunneling probability. Important parameters are extracted and tabulated for Si, Ge, GaAs, and GaSb, with a maximum error of $< 1.4\%$ compared to the numerical target.**

***Index Terms*—Band-to-band tunneling (BtBT), complex band structure, nonparabolicity.**

I. Introduction

THE EFFECT of band-to-band tunneling (BtBT) has attracted significant research interest due to its impact on device leakage in aggressively scaled MOSFETs as well as its potential application in tunneling devices to overcome the conventional "kT/q" limit of subthreshold swing [1]. Accurate modeling of BtBT probability in commonly used semiconductors presents a great challenge due to its extreme sensitivity to the electronic states in the bandgap region [3]–[5]. Theoretically, an electron travels in an evanescent decaying mode when it tunnels through a bandgap, resulting in a complex wavenumber along the tunneling direction. Accurate description of the energy dispersion of this complex wavenumber (i.e., complex band structure) is important not only to the improvement of numerical and compact modeling but also to the understanding of the tunneling physics itself. The past few decades have seen success in both the development of numerical methods for the calculation of complex band structures [5]–[8] and the application of the complex band theory to the modeling of tunneling devices [9]–[11]. Effort has also been made to attempt an analytical expression for the complex band branches in III–V materials [12]. However, a unified analytical expression remains to be found to accurately describe the complex band structures in commonly used direct- and indirect-gap semiconductors.

Manuscript received May 7, 2011; revised June 12, 2011; accepted June 14, 2011. Date of publication August 4, 2011; date of current version August 24, 2011. This work was supported in part by the Center for Energy Efficient Electronics Science, an NSF-funded Science and Technology Center, and in part by the member companies of the Initiative for Nanoscale Materials and Processes, Stanford University. The review of this letter was arranged by Editor L. Selmi.

The authors are with the Department of Electrical Engineering and Center for Integrated Systems, Stanford University, Stanford, CA 94305 USA (e-mail: ximeng@stanford.edu; dhkim81@gmail.com; saraswat@stanford.edu; hspwong@stanford.edu).

Color versions of one or more of the figures in this letter are available online at http://ieeexplore.ieee.org.

Digital Object Identifier 10.1109/LED.2011.2160143

In this letter, we show that the long-standing nonparabolic approximation (NPA) of real bands can be extended to describe the complex band structure of common semiconductor materials in the energy region important to BtBT. Compared to the capability to describe real bands, NPA shows even more improvement in describing the complex band structures over the parabolic approximation (PA). This is due to the inherent elliptic nature of the complex bands inside a bandgap region. With the recently developed numerical technique for complex band calculation [5], we have extracted and tabulated the NPA parameters for typical semiconductors. Comparison with PA shows a significant reduction of errors in the estimation of BtBT probability. The methodology is therefore suggested to be applicable in a broad range of materials and devices.

II. NPA

We start from Kane's two-band $k \cdot p$ model. Assuming that the conduction band minimum is at $k_0 = 0$, the electron Hamiltonian in the vicinity of k_0 is [2]

$$\begin{bmatrix} \frac{\hbar^2 k^2}{2m_0} & \frac{\hbar}{m_0} kp \\ \frac{\hbar}{m_0} kp^* & E_g + \frac{\hbar^2 k^2}{2m_0} \end{bmatrix} \tag{1}$$

where m_0 is the free electron mass, E_g is the energy bandgap, and $p = \langle u_{\mathrm{vk}_0} | \hat{p} | u_{\mathrm{ck}_0} \rangle$ is the momentum matrix element between two unit cell functions (u_{vk_0} and u_{ck_0}) at band extremes. Assume that $\hbar^2 k^2 / 2m_0$ is negligible compared to $E(k)$[1] and letting $E_p = 2|p|^2/m_0$, the secular equation is

$$E(k)\left[E(k) - E_g\right] = E_p \frac{\hbar^2 k^2}{2m_0}. \tag{2}$$

For $E(k) > E_g$, the conventional NPA of the conduction band can be obtained by defining $m^* = m_0 E_g / E_p$, $E'(k) = E(k) - E_g$, and $\alpha = 1/E_g$ [13]

$$E'(k)\left[1 + \alpha E'(k)\right] = \frac{\hbar^2 k^2}{2m^*}. \tag{3}$$

In practice, m^*, E_g, and α are fit to measurements or numerical results. For $E(k) \to E_g^+$, (3) degenerates into the PA (also known as effective-mass approximation) of the band, i.e., $E'(k) = \hbar^2 k^2 / (2m^*)$. Similar NPA of the valence band can be obtained from (2) for $E(k) < 0$.

[1]Keeping this term increases $E'(k)$ in (3) by $\hbar^2 k^2 / 2m_0$, which does not change the parabolic nature of the real band structure but only affects its curvature. Since in common semiconductors, m^* is much smaller than m_0, as shown in Table I, $\hbar^2 k^2 / 2m_0$ can be neglected as compared to $\hbar^2 k^2 / 2m^*$ in (3). The error induced in the curvature of the band is then mostly compensated by using a value of m^* fitted to the experimental data.

TABLE I
FITTED m_c AND m_v VALUES OF (5) AT Γ FOR THE DIRECT TUNNELING MODES OF Ge, GaAs, AND GaSb. VALENCE BRANCH OF Si IS ALSO FITTED FOR INDIRECT TUNNELING [19]

	$m_c(m_0)$	$m_v(m_0)$	$E_g^\Gamma(eV)$	Fit. Err.
Ge [100]	0.038	0.044	0.814	0.78%
Ge [110]	0.037	0.037	0.814	1.09%
Ge [111]	0.036	0.035	0.814	1.21%
GaAs [100]	0.064	0.072	1.416	0.96%
GaAs [110]	0.061	0.064	1.416	1.32%
GaAs [111]	0.061	0.062	1.416	1.40%
GaSb [100]	0.041	0.046	0.811	0.56%
GaSb [110]	0.039	0.041	0.811	0.76%
GaSb [111]	0.039	0.040	0.811	0.81%
Si [100]	0.370	0.201	3.398	0.29%
Si [110]	0.113	0.123	3.398	0.62%
Si [111]	0.121	0.109	3.398	0.66%

For BtBT, the energy of interest is within $0 < E(k) < E_g$. The solution of (2) therefore results in a complex k. Assuming that the electrons transport toward the positive direction so that the solution of (2) with a negative imaginary part (growing waves) can be safely discarded, we have $k = i\kappa$ with

$$\kappa = 1/\hbar\sqrt{2m^*E\left[1 - E/(2E_q)\right]} \tag{4}$$

and $E_q = E_g/2$. Unlike the situation in real band structures where only the band extremes determine current transport due to thermal statistics, the entire range of $0 < E(k) < E_g$ is of equal importance to the modeling of BtBT, since the electron has to traverse the entire bandgap to survive the tunneling process [5]. Equation (4) therefore reveals *the inherent elliptic nature of a complex band* which joins two real bands at their extremes. The key observations of (4) are the following.

1) In the limit of $E \to 0^+$: $\kappa \to 1/\hbar\sqrt{2m^*E}$ (PA of valence branch).
2) In the limit of $E \to E_g^-$: $\kappa = 1/\hbar\sqrt{2m^*E'[1 - E'/(2E_g - 2E_q)]} \to 1/\hbar\sqrt{2m^*E'}$, with $E' = E_g - E \to 0^+$ (PA of conduction branch).
3) $E(\kappa)$ and $d\kappa/dE$ are both continuous over $(0, E_g)$, and $d\kappa/dE|_{E_q} = 0$.

1) and 2) describe the asymptotic parabolic behavior of the complex bands near real band extremes, which agrees with PA. 3) instead is the unique feature of an ellipsoid, which defines the *branch point* E_q at which the conduction and valence branches join continuously [14].

For real band structures in which the electrons and holes have different effective masses, the simple two-band model in (1) may not hold. However, 1)–3) as well as the elliptic form of (4) serve as a guideline to construct the NPA of conduction and valence branches separately and join them smoothly. Taking the energy reference at the valence band maximum, the NPA of the complex branches in a direct bandgap is calculated in

$$\kappa_\Gamma = \begin{cases} \frac{1}{\hbar}\sqrt{2m_v E\left[1 - E/\left(2E_q^\Gamma\right)\right]}, & 0 < E < E_q^\Gamma \\ \frac{1}{\hbar}\sqrt{2m_c\left(E_g^\Gamma - E\right)\left[1 - \left(E_g^\Gamma - E\right)/\left(2E_g^\Gamma - 2E_q^\Gamma\right)\right]}, & E_q^\Gamma \le E < E_g^\Gamma \end{cases} \tag{5}$$

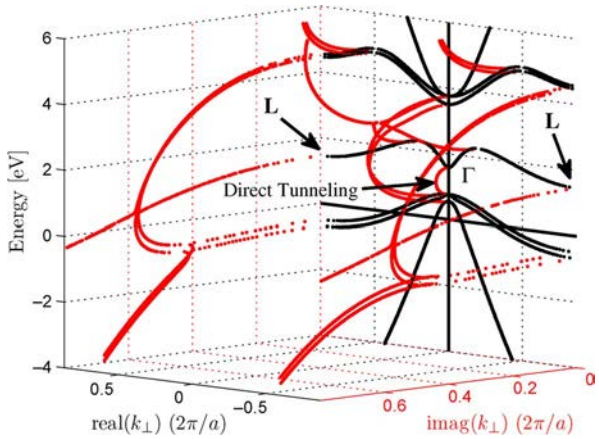

Fig. 1. (Color online) Complex band structures along [111] of bulk Ge. Black curves are the real band structure, while red curves are the complex branches. Aside from indirect branches from the L valleys, a direct tunneling branch exits at Γ.

TABLE II
FITTED PARAMETERS FOR (6). ENERGY REFERENCES FOR $E_{c\alpha}$ ARE AT THE VALENCE BAND MAXIMA. E_α IS THE ESTIMATED ENERGY DIFFERENCE BETWEEN VALENCE AND CONDUCTION STATES AT L (Ge) OR Δ (Si). ENERGY UNIT IS ELECTRONVOLTS [19]

	$m_c^\alpha(m_0)$	E_c^α	E_g^α	E_α	Fit. Err.
Ge@L [100]	0.116	0.678	1.081	1.940	0.24%
Ge@L [110]	0.080	0.678	1.035	1.940	0.16%
Ge@L [111]	0.090	0.678	0.993	1.940	0.12%
Si@Δ [100]	0.202	1.131	1.451	4.223	0.07%
Si@Δ [110]	0.185	1.131	2.865	4.223	1.27%
Si@Δ [111]	0.256	1.131	2.701	4.223	0.83%

with κ_Γ being the imaginary part of the wave vector, $m_v(m_c)$ being the hole (electron) effective mass, and E_g^Γ being the direct bandgap at Γ. $E_q^\Gamma = E_g^\Gamma m_c/(m_c + m_v)$ is the branch point which is obtained by imposing the continuity requirement on (5).

At indirect conduction band minima at $\mathrm{Re}\{\mathbf{k}\} = \mathbf{k}_\alpha$ (α being L for Ge and Δ for Si), only the conduction branch is within the energy of interest. The complex branch along the direction of interest is approximated as

$$\kappa_\alpha = \frac{1}{\hbar}\sqrt{2m_c^\alpha\left(E_c^\alpha - E\right)\left[1 - \left(E_c^\alpha - E\right)/\left(2E_\alpha - 2E_q^\alpha\right)\right]}, \quad E < E_c^\alpha \tag{6}$$

with $\kappa_\alpha = \mathrm{Im}\{k\}$, m_c^α being the electron effective mass, E_c^α being the energy minimum, E_q^α being the branch point at k_α, and E_α being the energy difference between conduction and valence states at k_α. Equations (5) and (6), both *elliptic* and *analytically integrable*, form the NPA of complex band structures within the energy region of interest.

III. COMPLEX BAND STRUCTURES

To verify the accuracy and applicability of NPA, the $sp^3d^5s^*$ tight-binding model [15]–[17] and a zone unfolding technique [18] are used to numerically generate complex band structures of semiconductors along selected orientations for comparison. For each orientation, the most relevant complex branches are selected as fitting target.

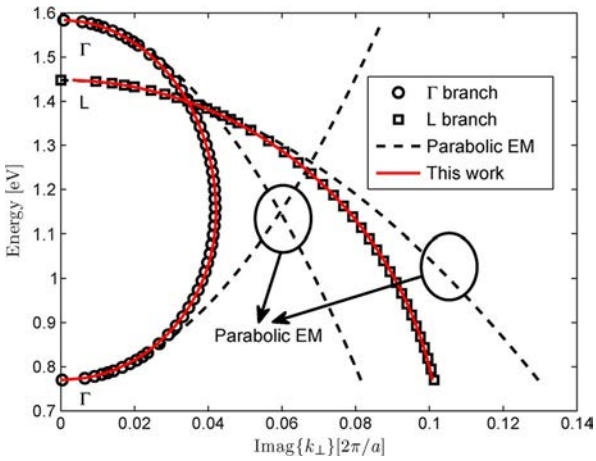

Fig. 2. Comparison between the parabolic and elliptic approaches in approximating the tunneling modes of Ge along [100]. Symbols are numerical results from the $sp^3d^5s^*$ tight-binding calculation [19].

IV. Results and Discussions

The numerically calculated complex band structure along [110] of bulk Ge is shown in Fig. 1. While the normal real band structure is shown by the gray curves on the $\mathrm{Im}\{k_\perp\} = 0$ plane, the black curves with imaginary wave vectors correspond to decaying (tunneling) modes along the transport direction $(\perp)$. Since the inverse of the BtBT probability (T) depends exponentially on the area of the region enclosed by the imaginary branch connecting the real band extremes (i.e., action integrals) [2], [4], it is observed that, aside from the indirect tunneling from Γ to L, a direct BtBT may dominate the current under strong bias condition, due to the small direct gap at Γ. Fig. 2 compares PA and NPA of the direct and indirect tunneling trajectories of Ge. NPA shows a satisfactory capability to be fit to numerical results. However, PA overestimates the action integral by 20% for direct tunneling and 30% for indirect tunneling, which translates to an underestimation of T by 70% and 80% when a constant field of 10^6 V/cm is present. To illustrate the implication of the NPA on the tunneling current calculation, we apply our NPA method together with a WKB approximation to a Ge diode. With the assumption of a triangular barrier and a built-in voltage of 0.8 V, a 0.1-V reverse bias leads to a direct BtBT current density of 218.2 kA/cm^2. A close result of 217.6 kA/cm^2 is obtained when the numerical tight-binding band structure is used. However, the application of PA leads to 159.7 kA/cm^2, revealing an underestimation by 26.63%. Similar errors are expected for indirect tunneling in Ge and tunneling in other materials. Tables I and II list the fitted parameters of (5) and (6) for Ge, GaAs, GaSb, and Si along different directions. The fitting errors are within 1.4% along all directions of these materials, which translates into a maximum error of T of less than 6% when a constant field of 10^6 V/cm is present. It is noted that the [110] direction has the smallest effective mass in both Si and Ge, because either Ge L ([1 −1 1]) or Si X ([001]) valleys have transverse effective mass along [110]. The largest effective mass, however, is along different directions in Ge ([100]) and Si ([111]), because along Ge [100] or Si [111], no valleys have transverse effective mass. The comparison of effective mass is therefore helpful to determine the optimal channel direction of a device.

V. Conclusion

An NPA has been constructed to capture the inherent elliptic nature of important complex band branches in semiconductors. The analytical form approaches the PA near band extremes, has a continuous derivative in the entire bandgap, and is integrable. The error of the BtBT probability is significantly reduced by this method compared to the PA. Although we have only used numerical tight-binding calculation as the fitting target, the elliptic form is expected to fit well to other empirical or first-principle results and is applicable to a wider range of materials with different band structures.

References

[1] A. C. Seabaugh and Q. Zhang, "Low-voltage tunneling transistors for beyond CMOS logic," *Proc. IEEE*, vol. 98, no. 12, pp. 2095–2110, Dec. 2010.
[2] E. O. Kane, "Zener tunneling in semiconductors," *J. Phys. Chem. Solids*, vol. 12, no. 2, pp. 181–188, Jan. 1960.
[3] M. Luisier and G. Klimeck, "Simulation of nanowire tunneling transistors: From the Wentzel–Kramers–Brillouin approximation to full-band phonon-assisted tunneling," *J. Appl. Phys.*, vol. 107, no. 8, p. 084507, Apr. 2010.
[4] D. Kim, "Theoretical performance evaluations of NMOS double gate FETs with high mobility materials: Strained III–V, Ge and Si," Ph.D. dissertation, Stanford Univ., Stanford, CA, 2009.
[5] S. E. Laux, "Computation of complex band structures in bulk and confined structures," in *Proc. 13th Int. Workshop Comput. Electron.*, 2009, pp. 1–2.
[6] J. K. Tomfohr and O. F. Sankey, "Complex band structure, decay lengths, and Fermi level alignment in simple molecular electronic systems," *Phys. Rev. B, Condens. Matter*, vol. 65, no. 24, p. 245 105, Jun. 2002.
[7] Y.-C. Chang, "Complex band structures of zinc-blende materials," *Phys. Rev. B, Condens. Matter*, vol. 25, no. 2, pp. 605–619, Jan. 1982.
[8] Y.-C. Chang and J. N. Schulman, "Complex band structures of crystalline solids: An eigenvalue method," *Phys. Rev. B, Condens. Matter*, vol. 25, no. 6, pp. 3975–3986, Mar. 1982.
[9] P. M. Solomon, S. E. Laux, L. Shi, J. Cai, and W. Haensch, "Experimental and theoretical explanation for the orientation dependence gate-induced drain leakage in scaled MOSFETs," in *Proc. Device Res. Conf.*, 2009, pp. 263–264.
[10] P. Mavropoulos, N. Papanikolaou, and P. H. Dederichs, "Complex band structure and tunneling through ferromagnet/insulator/ferromagnet junctions," *Phys. Rev. Lett.*, vol. 85, no. 5, pp. 1088–1091, Jul. 2000.
[11] P. Mavropoulos, "Spin injection from Fe into Si(001): Ab initio calculations and role of the Si complex band structure," *Phys. Rev. B, Condens. Matter*, vol. 78, no. 5, p. 054 446, Aug. 2008.
[12] C. Schnittler and M. Kirilov, "Two-band models for the complex band structure of III–V semiconductors," *Phys. Stat. Sol. (B)*, vol. 173, no. 2, pp. K19–K23, Oct. 1992.
[13] H. Flietner, "The $E(k)$ relation for a two-band scheme of semiconductors and the application to the metal–semiconductor contact," *Phys. Stat. Sol. (B)*, vol. 54, no. 1, pp. 201–208, Nov. 1972.
[14] J. Tersoff, "Schottky barrier heights and the continuum of gap states," *Phys. Rev. Lett.*, vol. 52, no. 6, pp. 465–468, Feb. 1984.
[15] J.-M. Jancu, R. Scholz, F. Beltram, and F. Bassani, "Empirical spds * tight-binding calculation for cubic semiconductors: General method and material parameters," *Phys. Rev. B, Condens. Matter*, vol. 57, no. 11, pp. 6493–6507, Mar. 1998.
[16] T. B. Boykin, G. Klimeck, and F. Oyafuso, "Valence band effective-mass expressions in the $sp^3d^5s^*$ empirical tight-binding model applied to a Si and Ge parametrization," *Phys. Rev. B, Condens. Matter*, vol. 69, no. 11, p. 115 201, Mar. 2004.
[17] T. B. Boykin, G. Klimeck, R. C. Bowen, and F. Oyafuso, "Diagonal parameter shifts due to nearest-neighbor displacements in empirical tight-binding theory," *Phys. Rev. B, Condens. Matter*, vol. 66, no. 12, p. 125 207, Sep. 2002.
[18] T. B. Boykin and G. Klimeck, "Practical applications of zone-unfolding concepts in tight-binding calculations," *Phys. Rev. B, Condens. Matter*, vol. 71, no. 11, p. 115 215, Mar. 2005.
[19] X. Guan, D. Kim, K. C. Saraswat, and H.-S. P. Wong, "Analytical approximation of complex band structures for band-to-band tunneling models," presented at the Int. Conf. Simulation Semiconductor Processes Devices (SISPAD), Osaka, Japan, 2011.